Isı Bilimi ve Tekniği Dergisi, 40, 2, 207-220, 2020
J. of Thermal Science and Technology

ISSN 1300-3615
https://doi.org/10.47480/isibted.816980

TURBULENT NATURAL CONVECTION AND RADIATION HEAT TRANSFER IN SQUARE ISOTROPIC SCATTERING MEDIUM

Mesut TEKKALMAZ
Eskisehir Osmangazi University, Department of Mechanical Engineering, Bati-Meselik, Eskisehir/TURKEY,
tmesut@ogu.edu.tr, ORCID: 0000-0003-3781-0384

(Geliş Tarihi: 28.01.2019, Kabul Tarihi: 16.04.2020)

Abstract: The influence of turbulent natural convection and thermal radiation in a differentially heated square enclosure is numerically investigated. The enclosure is heated from the right wall and cooled from the left wall. The other walls are assumed to be adiabatic. The Reynolds Averaged Navier Stokes (RANS) formulation was employed for analyzing turbulent flows together with a Realizable k–ε model. In addition, the discrete ordinates method (DOM) was used to solve the radiative transfer equation (RTE). Influence of Rayleigh number (Ra), optical thickness (τ), Planck number (Pl), scattering albedo (ω) and wall emissivity (ε_w) parameters were studied numerically on square enclosure for the flow and temperature distribution. It is interesting to note that a detailed parametric study focusing on characterizing parameters in turbulent natural convection and radiation was rarely dealt with in details. Solutions were obtained for a range of Rayleigh numbers varying from 10^9 to 10^{12}. It was found that the radiation heat transfer alters the characteristics of flow fields in the enclosure. Increasing the optical thickness results in a decrease in combined heat transfer for a fixed Rayleigh number and the maximum of heat transfer occurred for low optical thickness with radiation presence. $\overline{Nu_t}$ =87.796 and 82.351 is obtained for τ=0.2 and 5, respectively (Ra=10^{10}, Pl=0.02 and ω=0). The heat transfer increases with decreasing Planck number, and decreases with the increasing scattering albedo. $\overline{Nu_t}$ =445.837 and 68.100 is obtained for Pl=0.001 and 10, respectively (Ra=10^{10}, τ=1 and ω=0). When the active walls are black and the insulated walls are reflected, $\overline{Nu_t}$ =85.507 is obtained for Ra=10^{10}, Pl=0.02, τ=1 and ω=0.
Keywords: Turbulent natural convection, RANS, thermal radiation, isotropic scattering medium, square enclosure.

İZOTROPİK SAÇILMA ORTAMLI KARE GEOMETRİ İÇİNDE TÜRBÜLANSLI DOĞAL TAŞINIM VE IŞINIM ISI TRANSFERİ

Özet: Farklı ısıtılmış kapalı kare bir geometri içindeki türbülanslı doğal taşınım ve ısıl ışınımın etkisi sayısal olarak incelenmiştir. Kapalı kutu sağ duvardan ısıtılır ve sol duvardan soğutulur. Diğer duvarların adyabatik olduğu varsayılmaktadır. Reynolds Averaged Navier Stokes (RANS) formülasyonu, Realizable k–ε modeli ile birlikte türbülanslı akışları analiz etmek için kullanılmıştır. Ayrıca, ışınım transfer denklemini (RTE) çözmek için kesikli ordinatlar metodu (DOM) kullanılmıştır. Rayleigh sayısı (Ra), optik kalınlık (τ), Planck sayısı (Pl), saçılma albedosu (ω) ve duvar yayma oranı (ε_w) parametrelerinin etkisi, akış ve sıcaklık dağılımı kapalı kare geometri içinde sayısal olarak çalışılmıştır. Türbülanslı doğal taşınım ve ışınımda parametrelerin karakterize edilmesine odaklanan detaylı bir parametrik çalışmanın nadiren ayrıntılı olarak ele alındığını belirtmek ilginçtir. Çözümler 10^9 ila 10^{12} arasında değişen Rayleigh sayısı için elde edilmiştir. Işınım ısı transferinin geometri içinde akış alanlarının özelliklerini değiştirdiği bulunmuştur. Optik kalınlığın arttırılması, sabit bir Rayleigh sayısı için birleşik ısı transferinde bir azalmaya neden olurken ve ışınımla birlikte düşük optik kalınlıkta maksimum ısı transferi elde edilmiştir. τ=0.2 ve 5 için sırasıyla $\overline{Nu_t}$ =87.796 ve 82.351 elde edilmiştir (Ra=10^{10}, Pl=0.02 ve ω=0). Isı transferi azalan Planck sayısı ile artar ve artan saçılma albedo ile azalır. Pl=0.001 ve 10 için sırasıyla $\overline{Nu_t}$ =445.837 ve 68.100 bulunmuştur (Ra=10^{10}, τ=1 ve ω=0). Aktif duvarlar siyah, yalıtılmış duvarlar yansıtıcı olduğunda, Ra=10^{10}, Pl=0.02, τ=1 ve ω=0 için $\overline{Nu_t}$ =85.507 elde edilmiştir.
Anahtar Kelimeler: Türbülanslı doğal taşınım, RANS, Isıl ışınım, İzotropik saçılmalı ortam, Kare geometri

NOMENCLATURE

a	absorption coefficient, [m^{-1}]
c_p	specific heat capacity, [J/kg K]
C_μ	constant in the k–ε models
g	acceleration due to gravity, [m/s^2]
I	radiation intensity, [W/m^2]
k	turbulent kinetic energy, [m^2/s^2]

L	enclosure height and weight, [m]
n	refractive index
Nu	Nusselt number,
P	pressure, [Pa]
Pl	Planck number, $[=(\lambda / L)/(4\sigma T_0^3)]$
Pr	Prandtl number, $[=\nu/\alpha]$
q	heat flux, [W/m^2]
$\mathbf{r}$	position vector
Ra	Rayleigh number, $[=g\beta(T_h - T_c)L^3/(\nu\alpha)]$
$\mathbf{s}$	direction vector
$\mathbf{s}'$	scattering direction vector
S	modulus of the mean rate-of-strain tensor
S_{ij}	mean rate of strain tensor
t	time, [s]
T	temperature, [K]
T_c	temperature of cold wall, [K]
T_h	temperature of hot wall, [K]
T_0	reference temperature, $[=(T_h + T_c)/2$, K]
u, v	horizontal and vertical velocity components, [m/s]
U	dimensionless horizontal velocity components, $[=u/(\alpha Ra^{1/2}/L)]$
V	dimensionless vertical velocity components, $[=v/(\alpha Ra^{1/2}/L)]$
x, y	cartesian coordinates, [m]
X,Y	dimensional coordinates, [$X=x/L$, $Y=y/L$]

Greek letters

α	thermal diffusivity, [m/s^2]
β	coefficient of thermal expansion, [1/K]
λ	thermal conductivity, [W/mK]
δ_{ij}	Kronecker delta
ΔT	temperature difference, $[=(T_h - T_c)$, K]
ε_w	wall emissivity
ε	dissipation rate of k, $[m^2/s^3]$
θ	dimensionless temperature, $[=(T - T_o)/(T_h - T_c)]$
θ_0	reference temperature ratio, $[=T_o/(T_h - T_c)]$
ν	kinematic viscosity, [m^2/s]
ω	scattering albedo, $[=\sigma_s/(a+\sigma_s)]$
μ	dynamic viscosity, [kg/m s]
μ_t	turbulent eddy viscosity, [kg/m s]
ρ	density, [kg/m^3]
σ	Stefan Boltzmann constant, [W/m^{2}K^4]
σ_s	scattering coefficient, [m^{-1}]
σ_T	turbulent Prandtl number
τ	optical thickness, $[=(a+\sigma_s)L]$
Φ	phase function
Ω'	solid angle

Subscripts

c	convection, cold
h	hot
i,j	elemental directions (i, j = 1 and 2 corresponding to the x and y directions)
r	radiation
t	total
w	wall
w1,w2 w3,w4	right wall, left wall, bottom wall, top wall

Abbreviations

DOM	Discrete Ordinates Method
DNS	Direct Numerical Simulation
LES	Large Eddy Simulation
LBM	Lattice Boltzmann Method
P_1	Spherical Harmonics Method
PRESTO	Pressure Staggering Option
RANS	Reynolds Averaged Navier Stokes
RNG	Renormalization Group
RTE	Radiative Transfer Equation

INTRODUCTION

Analysis of natural convection and radiation in participating media is an important process in various engineering systems such as the design of furnaces, heat exchangers, cooling of electronic devices and nuclear reactors, spacecraft, thermal insulation, heat buildings, the metallurgy and solar capture, and so on. In these and similar engineering applications, radiation can strongly interact with convection. The variation of flow and temperature distribution is directly influenced by the radiation effects. In fact, the effects on the flow and heat transfer of parameters as Rayleigh number, Planck number, wall emissivity and the scattering albedo are present in several engineering applications in industry.

Studies on the interaction of radiation and laminar natural convection heat transfer began in the 80's. Lauriat (1982) studied a two-dimensional vertical cavities of different optical thickness, whereas P_1 (Spherical Harmonics Method) gray gas method was used for various formulation and analyzed non-gray gas radiation characterized by the radiation band structure. Also Desrayaud and Lauriat (1985) extended the study of a fluid layer of the vertical wall. Webb and Viskanta (1987) examined the rate of internal radiative heating on the natural convective motion in a vertical rectangular enclosure irradiated from the side wall. Fusegi and Farouk (1989) studied numerically the interactions of laminar and turbulent natural convection and gray gas radiation in a differentially heated square enclosure and used P_1 approximation method for solving the radiative transfer equation (RTE). The numerical investigation of interactions of natural convection and radiation in a square enclosure was performed by Yucel et al. (1989). They used Discrete Ordinates Method (DOM) to solve the RTE. Also these same authors analyzed the changes in the buoyant flow patterns and temperature distributions due to the presence of radiation in inclined or heat generating enclosures (Yucel et al., 1994). In the same trend Draoui et al. (1991) used the P_1 method to analyze the effects of radiation and natural convection on the heat transfer process in a square enclosure. Tan and Howell (1991) studied the combined radiation and laminar natural convection in a two-dimensional

participating square medium numerically. They found that the radiation destroyed the symmetry of the flow structure and temperature field.

These mentioned studies have been dealt with different solution methods in the last decade. Mezrhab et al. (2008) performed the numerical study of double-diffusion convection coupled to radiation in a square cavity filled with absorbing, emitting and non-scattering gray gas. They modeled the RTE by the DOM method. Mondal and Mishra (2009) analyzed the simulation of natural convection in the presence of thermal radiation using the lattice Boltzmann method (LBM). In this study, they investigated the effects of the extinction coefficient and the scattering, albedo on flow field and temperature distribution. Moufekkir et al. (2012) studied numerically the laminar natural convection and thermal radiation in an isotropic scattering medium within a heated square cavity using a hybrid thermal lattice Boltzmann method. They later investigated the effect of the inclination angle of enclosure on heat transfer in the similar problem (Moufekkir et al, 2012).

Coupled turbulence natural convection and radiation in differentially heated cavity was investigated by many researches. In general, turbulent flows have been investigated using three numerical approximation techniques: Direct Numerical Simulation (DNS), Large Eddy Simulation (LES) and RANS. Using the DNS turbulence method, combined turbulence natural convection and radiation in a 2D and 3D enclosures are considered in the literature (Salat et al., 2004; Xin et al., 2004; Sergent et al., 2013; Soucasse et al., 2014; Czarnota and Wagner, 2016). Commonly, there are many studies considering the interaction of turbulence models and thermal radiation at low Rayleigh number in LES method (Capdevila et al., 2011; Capdevila et al., 2012; Ibrahim et al., 2013).

Among RANS models, the standard k–ε model has been adopted by many authors. Mesyngier and Farouk (1996) examined the combined turbulent natural convection and radiation in a 2D differentially heated square cavity filled with a single participating gas or a homogeneous mixture of two participating gases along with a non-participating gas. The interaction of surface radiation with turbulent natural convection of a transparent medium in 2D square and tall enclosures was analyzed by Velusamy et al. (2001). In this study, the enclosure isolated from the horizontal walls heated from the vertical walls was changed to Ra 10^9–10^{12} and aspect ratio 1-200. Sharma et al. (2007) investigated the interaction of surface radiation with turbulent natural convection of a transparent medium in a rectangular enclosure heated from below and cooled from the other three walls with the Rayleigh number varying from 10^8 to 10^{12} and the aspect ratio changing from 0.5 to 2.0. The same authors analyzed the same geometry with the inclination angle varying between 0°-90° and Rayleigh numbers from 10^8 to 10^{12} (Sharma et al., 2008). Shati et al. (2012) presented the effect of turbulence natural convection with and without the interaction of surface radiation in 2D square and rectangular enclosures, using the renormalization group (RNG) k–ε model. Xaman et al. (2008) studied numerically the combined heat transfer (laminar and turbulent natural convection, surface thermal radiation and conduction) in a square cavity with a glass wall. Wu and Lie (2015) numerically investigated turbulent natural convection with and without radiation transfer in 2D and 3D air-filled differentially heated cavities using various RANS models. They compared two equation eddy-viscosity models which are the standard k–ε model, RNG k–ε model, the realizable k–ε model, the standard k–ω model and the shear-stress transport (SST) k–ω model. The numerical analysis of conjugate turbulent natural convection combined with the surface thermal radiation in an enclosure has been carried out by Miroshnichenko et al. (2015), Sheremet and Miroshnichenko (2015).

The scattering albedo, the Planck number and the surface emissivity effects for participating and isotropically scattering media were rarely studied in detail for high Rayleigh number. Since these parameter effects find their use in several industrial processes for various ranges, the objective of the present study is to simulate turbulence natural convection in a two dimensional square enclosure in the presence of thermal radiation. Also, the performance of the realizable k–ε turbulence model and DOM method are investigated in natural convection with radiation in an enclosure for the effect of various influencing parameters such as the Rayleigh number, the Planck number, the scattering albedo and the surface emissivity.

GOVERNING EQUATIONS

The geometry of a two-dimensional square enclosure is shown in Fig. 1. The physical model consists of a gray, absorbing, emitting, and isotropically scattering fluid in a square enclosure surrounded by the walls. Two horizontal walls are insulated, and two vertical isothermal walls are kept at temperatures, T_h=1000K and T_c=500K, respectively. The cavity is filled with a Newtonian fluid of Pr=0.71. All physical properties in the system are assumed to be constant for T_0 reference temperature, expect for the density. The radiating fluid is assumed to be incompressible; viscous dissipation is neglected.

The continuity and unsteady Reynolds-averaged Navier Stokes and energy equations (in tensor notation) for the buoyancy-excited turbulent air flow within the enclosure can be written as follows with Boussinesq assumption:

$$\frac{\partial u_i}{\partial x_i} = 0 \tag{1}$$

$$\rho\frac{\partial u_i}{\partial t}+\rho u_j\frac{\partial u_i}{\partial x_j}= -\frac{\partial P}{\partial x_i}+\frac{\partial}{\partial x_j}\left[\mu\left(\frac{\partial u_i}{\partial x_j}+\frac{\partial u_j}{\partial x_i}\right)-\rho\overline{u_i'u_j'}\right]-g_i\beta(T-T_0) \quad (2)$$

$$\rho c_p\frac{\partial T}{\partial t}+\rho c_p\frac{\partial (u_jT)}{\partial x_j}=\frac{\partial}{\partial x_j}\left[\lambda\frac{\partial T}{\partial x_j}-\rho\overline{u_i'T'}\right]-\nabla\cdot\mathbf{q}_r \quad (3)$$

where x_i and x_j are the Cartesian coordinates in the i and j directions, t is the time, P is the pressure, T is the time averaged temperature, T_0 is the reference temperature, u_i and u_j are the time averaged velocity components in the i and j directions, u_i' and u_j' are the corresponding unstable velocity components in the i and j directions, ρ is the fluid density, λ is the thermal conductivity, c_p is the specific heat capacity, and μ is the dynamic viscosity.

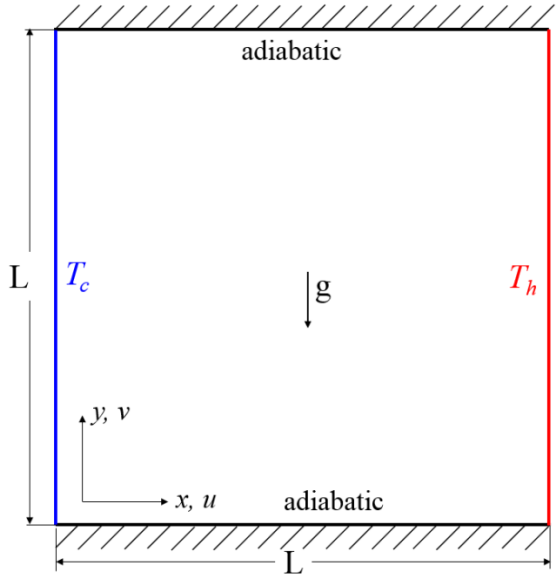

Figure 1. Schematic geometry of the problem.

The Reynolds stresses ($-\rho\overline{u_i'u_j'}$) and the turbulence heat fluxes ($\overline{u_i'T'}$) need to be modeled in order to solve Eq (1) and (3). The Reynolds stresses are modeled through the Boussinesq approximation as:

$$-\rho\overline{u_i'u_j'}=\mu_t\left(\frac{\partial u_i}{\partial x_j}+\frac{\partial u_j}{\partial x_i}\right)-\frac{2}{3}\rho k\delta_{ij} \quad (4)$$

where μ_t is the turbulent eddy viscosity, k is the turbulent kinetic energy, δ_{ij} is the Kronecker delta ($\delta_{ij}=0$ if $i\neq j$ and $\delta_{ij}=1$ if $i=j$). The turbulent eddy viscosity is obtained by

$$\mu_t=\frac{\rho c_\mu k^2}{\varepsilon} \quad (5)$$

In this study, two equations the realizable k-ε model is considered. The difference between the realizable k-ε model and the standard and RNG k-ε models is that C_μ is no longer constant:

$$C_\mu=\frac{1}{4.04+\sqrt{6}\cos\phi\left(kU^*/\varepsilon\right)} \quad (6)$$

where

$$U^*=\sqrt{S_{ij}S_{ij}+\tilde{\Omega}_{ij}\tilde{\Omega}_{ij}},\quad \tilde{\Omega}_{ij}=\Omega_{ij}-2\varepsilon_{ijk}\omega_k,$$
$$\Omega_{ij}=\overline{\Omega}_{ij}-2\varepsilon_{ijk}\omega_k$$
$$\phi=\frac{1}{3}\cos^{-1}\left(\sqrt{6}W\right),\quad W=\frac{S_{ij}S_{jk}S_{ki}}{\tilde{S}},\quad \tilde{S}=\sqrt{S_{ij}S_{ij}}, \quad (7)$$
$$S_{ij}=\frac{1}{2}\left(\frac{\partial u_j}{\partial x_i}+\frac{\partial u_i}{\partial x_j}\right)$$

$\overline{\Omega}_{ij}$ is the mean rate of rotation tensor viewed in a rotating reference frame with the angular velocity ω_k. Also ε_{ijk} is discretized by using Eq. (13).

$$\overline{u_i'T'}=-\frac{\mu_t}{\rho\sigma_T}\frac{\partial T}{\partial x_i} \quad (8)$$

where σ_T is the turbulent Prandtl number.
The turbulent kinetic energy (k), is as follows assuming incompressible flow and no source terms:

$$\frac{\partial(\rho k)}{\partial t}+\frac{\partial\left(\rho k u_j\right)}{\partial x_j}= \frac{\partial}{\partial x_j}\left(\left(\mu+\frac{\mu_t}{\sigma_k}\right)\frac{\partial k}{\partial x_j}\right)+G_k+G_b-\rho\varepsilon \quad (9)$$

where G_k represents the production of turbulent kinetic energy, which is common to all k-ε turbulence models and is given by

$$G_k=-\overline{u_i'u_j'}\frac{\partial u_j}{\partial x_i} \quad (10)$$

The term G_b represents the generation of turbulent kinetic energy because of buoyant forces when the system is under a gravitational field, and it is calculated as follows:

$$G_b=\beta g_i\frac{\mu_t}{\mathrm{Pr}_t}\frac{\partial T}{\partial x_i} \quad (11)$$

where Pr_t= 0.85 is the Prandtl number for energy and β is the thermal expansion coefficient, which is calculated as follows:

$$\beta=-\frac{1}{\rho}\left(\frac{\partial\rho}{\partial T}\right)_P \quad (12)$$

Turbulent dissipation rate (ε), is as follows assuming incompressible flow and no source terms:

$$\frac{\partial(\rho\varepsilon)}{\partial t}+\frac{\partial\left(\rho\varepsilon u_j\right)}{\partial x_j}=\frac{\partial}{\partial x_j}\left(\left(\mu+\frac{\mu_t}{\sigma_\varepsilon}\right)\frac{\partial\varepsilon}{\partial x_j}\right) +\rho C_1 S\varepsilon-\rho C_2\frac{\varepsilon^2}{k+\sqrt{\nu\varepsilon}}+C_{1\varepsilon}\frac{\varepsilon}{k}C_{3\varepsilon}G_b \quad (13)$$

where,

$$C_1 = \max\left[0.43, \frac{\eta}{\eta+5}\right], \quad \eta = S\frac{k}{\varepsilon},$$
$$S = \sqrt{2S_{ij}S_{ij}}, \qquad C_{3\varepsilon} = \tanh\left|\frac{u_j}{u_i}\right| \tag{14}$$

and σ_k and σ_ε are the turbulent Prandtl numbers for k and ε, respectively. The constants used in the realizable k-ε model are as follows:

$$\sigma_k = 1, \quad \sigma_\varepsilon = 1.2, \quad C_{1\varepsilon} = 1.44, \quad C_2 = 1.9 \tag{15}$$

The local divergence of radiative flux $\nabla \cdot \mathbf{q}_r$ in the energy equation is related to the local intensities by:

$$\nabla \cdot q_r = a\left(4\pi I_b(\mathbf{r}) - \int_{4\pi} I(\mathbf{r},\Omega)d\Omega\right) \tag{16}$$

To obtain the radiation intensity field and $\nabla \cdot \mathbf{q}_r$, it is necessary to solve the RTE.

The DOM model solves the radiative transfer equation over a finite number of solid angles, each associated with a vector direction ***s*** in the global Cartesian system (x, y). The DOM model does not perform ray tracing. Instead, the RTE is transformed into as many transport equations as there are solid angles with direction ***s***. The solution method is the same as that used for the momentum and energy equations. The RTE in the direction ***s*** can be written as follows:

$$\nabla \cdot (I(\mathbf{r},\mathbf{s})\mathbf{s}) + (a+\sigma_s)I(\mathbf{r},\mathbf{s}) = an^2\frac{\sigma T_0^4}{\pi} + \frac{\sigma_s}{4\pi}\int_0^{4\pi} I(\mathbf{r},\mathbf{s})\Phi(\mathbf{s}\cdot\mathbf{s}')d\Omega' \tag{17}$$

where, **r** is position vector**,** **s** is direction vector, $\mathbf{s}'$ is scattering direction vector, s is path length, a is absorbing coefficient, n is refractive index, σ_s is scattering coefficient, σ is Stefan-Boltzmann constant, I is radiation intensity, Φ is phase function and Ω' is solid angle.

The boundary conditions are as follows:

$$\begin{aligned} &u_i = 0, \quad \text{at all walls} \\ &T = T_c, \quad 0 \le y \le L \ \text{ and } x = 0 \\ &T = T_h, \quad 0 \le y \le L \ \text{ and } x = L \\ &q_c + q_r = 0, \ \text{at the adiabatic wall (top and bottom)} \end{aligned} \tag{18}$$

The radiative heat flux on boundary surfaces (q_r) can be expressed as;

$$q_r = \varepsilon_w\left(\pi I_b(r_w) - \int_{\mathbf{n}\cdot\mathbf{s}'<0} I(r_w,\mathbf{s}')|\mathbf{n}\cdot\mathbf{s}'|d\Omega\right) \tag{19}$$

and the radiative boundary condition for diffusely reflecting surfaces in Eq. (19) is

$$I(r_w,\mathbf{s}) = \varepsilon_w I_b(r_w) + \frac{1-\varepsilon_w}{\pi}\int_{\mathbf{n}\cdot\mathbf{s}'<0} I(r_w,\mathbf{s}')|\mathbf{n}\cdot\mathbf{s}'|d\Omega \tag{20}$$

where **n** is the outward normal at the boundary.

The total wall heat flux is calculated as

$$q_t = q_c + q_r \tag{21}$$

where q_c and q_r are the convective and radiative heat flux at wall, calculated as

$$q_c = -\lambda\frac{\partial T}{\partial n} \quad \text{and} \quad q_r = \int_{4\pi} I(\mathbf{n}\cdot\mathbf{s})|_w d\Omega \tag{22}$$

The total Nusselt number at the walls are calculated from the convective and radiative Nusselt number as

$$Nu_t = Nu_c + Nu_r = \frac{q_c L}{\lambda(T_h - T_c)} + \frac{q_r L}{\lambda(T_h - T_c)} \tag{23}$$

The mean Nusselt number $\overline{Nu}$ at the wall is the line averaged value of *Nu*.

NUMERICAL SOLUTION

In this study, Fluent (2011) was used to numerically simulate the existing problem. The unsteady continuity, RANS and energy equations are discretized by employing finite volume and the resulting equations are iteratively solved. The computational domain is divided non uniform finite volumes using structured cells. A second order time implicit scheme is adopted to apply solution. The PRESTO (Pressure Staggering Option) scheme is employed for pressure term while The second order upwind scheme is adopted for the others. Further, the pressure velocity coupling is implemented based on SIMPLE algorithm. For the radiation transfer, the DOM is used. The angular resolution is 4x6. The two-layer model (Enhanced Wall Treatment model) is used to achieve near wall modeling approach. Additionally, the thermal effects and the full buoyancy effect options in the related turbulence models were activated. The convergence criteria imposed to all of the equation was 10^{-5}. The time-dependent approach is used to obtain the steady-state solution. To determine the time step size, the criteria, $\Delta t \approx L/(4\sqrt{g\beta\Delta TL})$ as, recommended by Fluent (2011).

For the validation of the problem, the turbulence natural convection of CO_2 radiation interaction in square enclosure has been solved Rayleigh values of 10^8, 10^9 and 10^{10}. This problem was studied numerically by Fusegi and Farouk (1989), Mesyngier and Farouk (1996). In all cases, the enclosure was considered to be filled with CO_2 at atmospheric pressure. The reference temperature T_0 is 555 K, and the wall temperatures are T_c = 277.5 K and T_h = 832.5 K. The corresponding Pl for these cases is 0.0046, 0.0021 and 0.001, while τ varies from 0.1443 to 0.191. Figure 2 shows mean total Nusselt numbers as a function of Ra for the above conditions. The numerical solution depicts very good agreement those of published results.

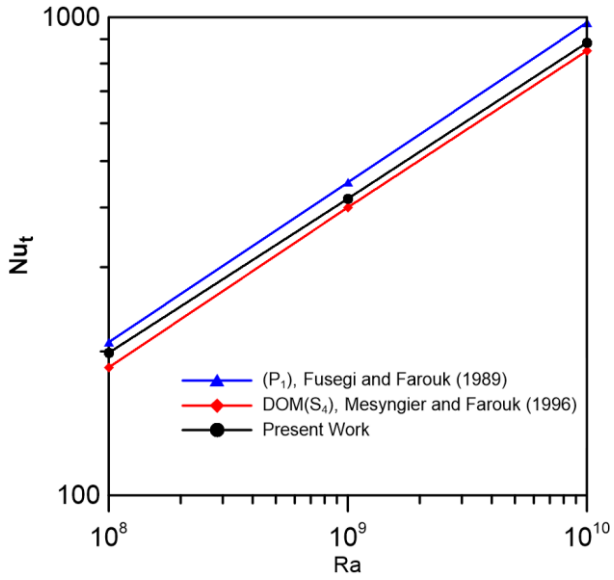

Figure 2. Comparison of P_1, DOM (S4) and present work for mean Nusselt number as a function of Ra.

A second validation problem is the turbulence natural convection of air surface radiation interaction in a square enclosure at Rayleigh number of 1.5×10^9. The comparisons of numerically obtained mean Nusselt numbers relative to experimental measurement and numerical are given in Table 1. According to the experimental result, the maximum relative error is 6.31%.

Table 1. Comparison of mean convective Nusselt number for $Ra=1.5\times10^9$ and $\tau=0$.

Models	$\overline{Nu_c}$	Error relative to Experimental Data
Experiment (Salat et al., 2004)	54	
SST k–ω (Wu and Lei, 2015)	56.18	4.04
Present Work (Realizable k-ε)	57.41	6.31

Table 2. Comparison of mean total, radiative and convection Nusselt number on hot wall various grid sizes for $Ra=10^9$, Pl=0.02, ω=0 and $\varepsilon_{w1}=\varepsilon_{w2}=\varepsilon_{w3}=\varepsilon_{w4}=1$.

	$\overline{Nu_t}$	$\overline{Nu_r}$	$\overline{Nu_c}$	Grid
τ=0.2	56.588	26.801	29.787	100×100
	56.454	26.786	29.668	200×200
	56.448	26.786	29.662	400×400

Table 2 presents the mean convection, radiation and total Nusselt numbers for different grid values for $Ra=10^9$, Pl=0.02 and ω=0. Variation in the number of grid points from 200×200 with stretching ratio 1.05 to 400×400 with stretching ratio 1.05 affects the mean total, radiative and convection Nusselt number by less than 0.01%, 0.0% and 0.02%, respectively. Numerical accuracy was further checked by refining the grid so that wall $y^+ << 1$ in computations. Turbulence solution of the mesh is given in Fig.3. The grid size of 400×400 cells is therefore chosen for all cases studies (Fig. 3).

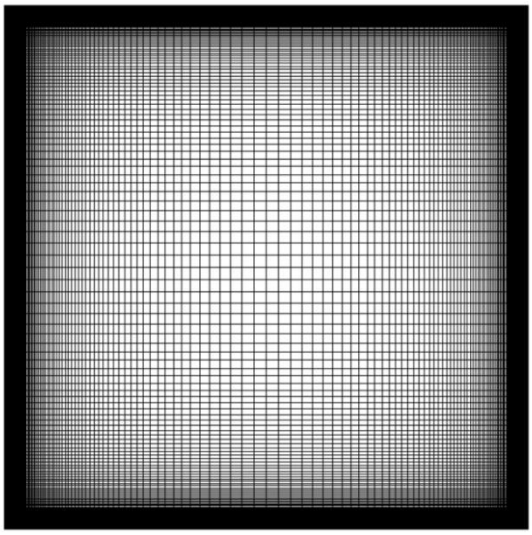

Figure 3. Unstructured grid system for enclosure.

RESULTS AND DISCUSSION

The differentially heated square enclosure and filled with an isotropic scattering medium as illustrated in Fig. 1. In this study, the Prandtl number was fixed at Pr=0.71, the other parameters such as Rayleigh number, Planck number, the scattering albedo and wall emisivity were varied in order to quantify their effects on the heat transfer and the fluid flow in the enclosure. The Planck number expresses the relationship between heat transfer by conduction and radiation. The reference temperature ratio θ_0 is considered equal to 1.5 and the ratio T_c/T_h is fixed at 0.5, under the Boussinesq approximation. This approximation is accurate as long as changes in actual density are small; specifically, the Boussinesq approximation is valid when $\beta(T-T_0)<<1$ (Fluent, 2011).

Optical Thickness and Rayleigh Number Effects

In Figure 4, the isotherms (left) and the streamlines (right) are depicted at $Ra=10^{10}$, Pl=0.02 and ω=0 for various the optical thicknesses (τ=0.2, 1 and 5). In case of τ=0 (surface radiation), the isotherms and the streamlines exhibit nearly centro symmetric structure that are characterized by the formation of extremely thin boundary layers along the isothermal walls and a thermally stratified. As the optical thickness increases with the presence of radiation, the centrosymmetric of the streamline deteriorates, but there is no change in the thermally stratified in the isotherms. Indeed, the optical thickness increase slightly changes the temperatures distribution.

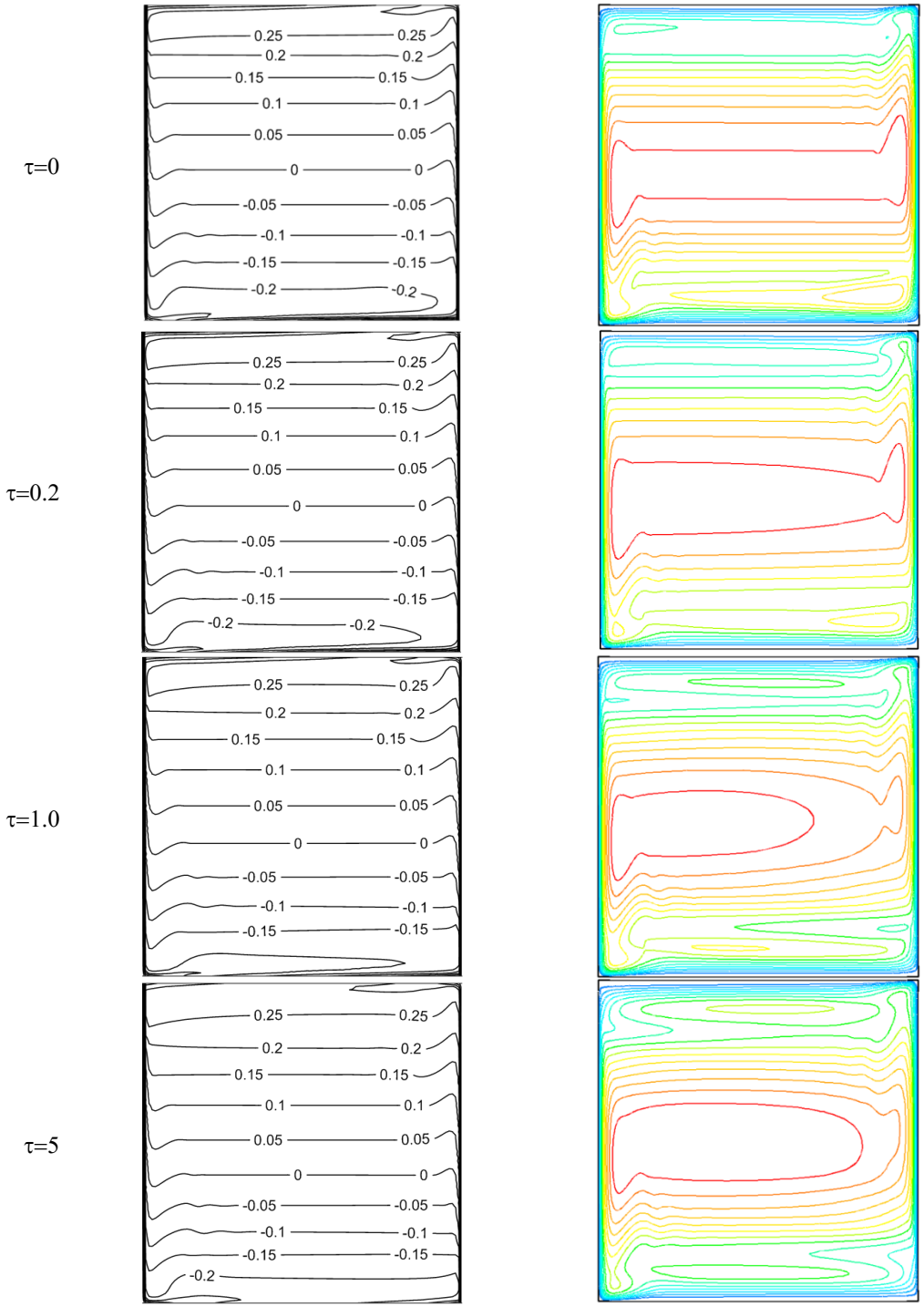

Figure 4. Isotherms (left) and streamlines (right) at Ra=10^{10}, Pl=0.02, ω=0, for $\varepsilon_{w1}=\varepsilon_{w2}=\varepsilon_{w3}=\varepsilon_{w4}=1$.

Figure 5 shows the temperature profiles along the respective horizontal and vertical mid-planes. Thermal radiation causes the temperature to rise slightly. While the optical thickness increases, the temperature profiles become similar. Large temperature gradients are observed near the hot and cold walls. In addition, an increase in temperature indicates that the medium participates more and the radiation effect is stronger and the convection effect is weakened. In the case no radiation, the vertical and horizontal gradients of temperature are much lower than those of the other. In the presence of both transparent and participating medium, the fluid heats up very quickly when it approaches the hot wall, and cools down very quickly when it approaches the cold wall.

Figure 6 displays the vertical and horizontal velocity profile along the respective horizontal and vertical mid-planes. The horizontal velocity gradients vary considerably in the region near the insulated horizontal plates by the radiation. Similarly, the vertical velocity gradients show a sharp change in the region near the thermally active walls. At the same time the flow in the enclosure is almost stagnant, forming a distinct core region and boundary layer structures is located in regions adjacent to the hot and cold walls.

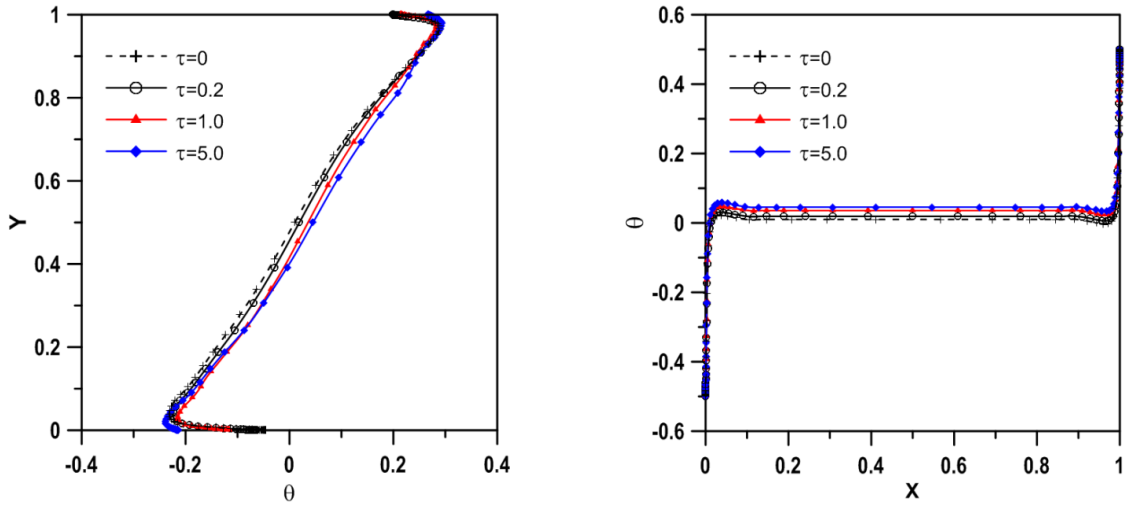

Figure 5. Temperature distribution at X=0.5 mid-plane (left) and Y=0.5 mid-plane (right) for Ra=10^{10}, Pl=0.02, ω=0, $\varepsilon_{w1}=\varepsilon_{w2}=\varepsilon_{w3}=\varepsilon_{w4}=1$.

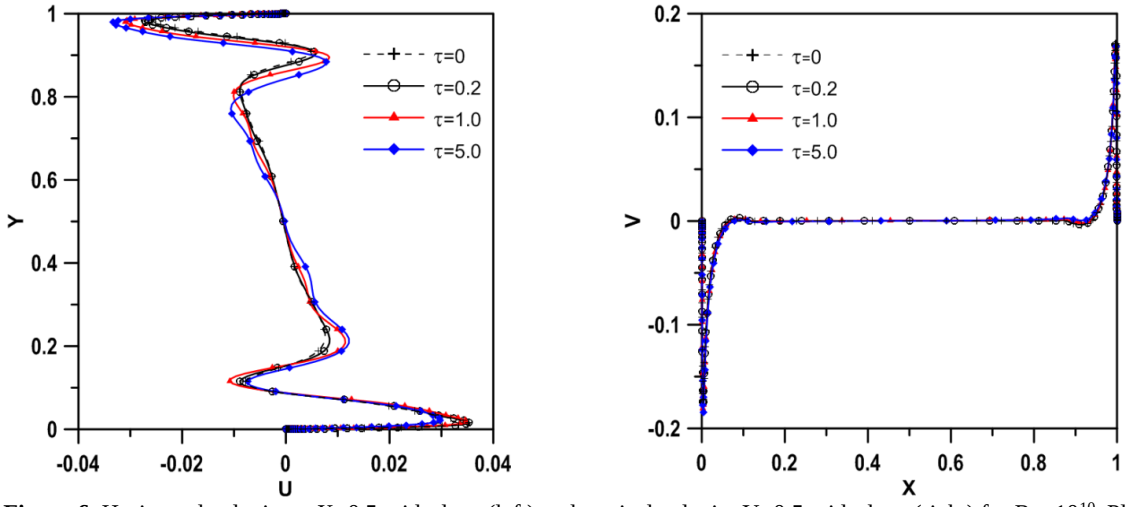

Figure 6. Horizontal velocity at X=0.5 mid-plane (left) and vertical velocity Y=0.5 mid-plane (right) for Ra=10^{10}, Pl=0.02, ω=0, $\varepsilon_{w1}=\varepsilon_{w2}=\varepsilon_{w3}=\varepsilon_{w4}=1$.

Figure 7 depicts the variation of the mean total Nusselt number ($\overline{Nu_t}$) for various optical thicknesses and for different the Rayleigh numbers. In both surface radiation (τ=0) and thermal radiation (τ=0.2,1,5), the $\overline{Nu_t}$ increases with increasing Rayleigh number and decreases with increasing optical thickness. With increasing Rayleigh number, the buoyancy forces will increasingly play a major role in heat transfer across the enclosure. With increasing optical thickness, the radiative flux exchanged between the enclosure walls decreases slightly. Therefore, the maximum of heat transfer is achieved at low optical thickness.

The variations of the mean total and radiative Nusselt numbers as functions of Rayleigh number, the scattering albedo and the optical thickness are shown in Table 3. When the optical thickness and scattering albedo are constant, the mean total and radiative Nusselt numbers increase with the Rayleigh number. Besides, when the scattering albedo and the Rayleigh number remain constant, $\overline{Nu_t}$ and $\overline{Nu_r}$ decrease as the optical thickness increases.

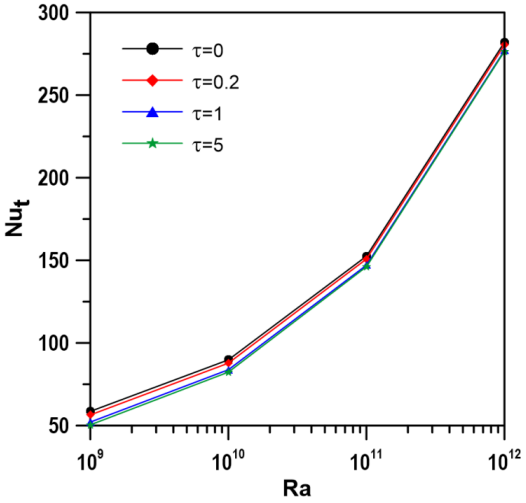

Figure 7. Mean total Nusselt number versus Rayleigh number for various optical thicknesses with Pl=0.02, ω=0 and $\varepsilon_{w1}=\varepsilon_{w2}=\varepsilon_{w3}=\varepsilon_{w4}=1$.

Table 3. Variation of the mean total, radiative and convection Nusselt number according to scattering albedo for different values of Rayleigh number and optical thicknesses ($\varepsilon_{w1}= \varepsilon_{w2}= \varepsilon_{w3}= \varepsilon_{w4}=1$).

			10^9	10^{10}	10^{11}	10^{12}
τ=0.2	ω=0	$\overline{Nu_t}$	56.448	87.796	150.797	280.376
		$\overline{Nu_r}$	26.786	27.472	28.040	28.423
	ω=0.5	$\overline{Nu_t}$	56.439	87.508	150.706	280.266
		$\overline{Nu_r}$	26.231	26.883	27.435	19.994
	ω=1.0	$\overline{Nu_t}$	56.441	87.711	150.611	280.116
		$\overline{Nu_r}$	25.550	26.186	26.733	27.120
τ=1.0	ω=0	$\overline{Nu_t}$	52.141	83.807	147.062	277.042
		$\overline{Nu_r}$	24.894	25.303	26.073	26.591
	ω=0.5	$\overline{Nu_t}$	51.540	83.230	146.595	276.372
		$\overline{Nu_r}$	22.615	23.480	24.160	24.603
	ω=1.0	$\overline{Nu_t}$	50.854	82.390	145.581	275.267
		$\overline{Nu_r}$	19.628	20.318	20.920	21.346
τ=5.0	ω=0	$\overline{Nu_t}$	50.429	82.351	146.137	276.525
		$\overline{Nu_r}$	22.238	23.811	24.913	25.629
	ω=0.5	$\overline{Nu_t}$	48.303	80.415	144.259	274.402
		$\overline{Nu_r}$	19.573	20.799	21.652	22.207
	ω=1.0	$\overline{Nu_t}$	42.510	74.442	137.979	267.923
		$\overline{Nu_r}$	10.010	10.570	11.053	11.441

Planck Number Effects

The effect of the Planck number in presence of radiation is applied for $Ra=10^{10}$, ω=0 and τ=1. The radiation will dominate when the Planck number is low. Figure 8 illustrates the effect of Planck number on isothermal contours (top) and the streamlines (bottom). For Pl=0.001, the radiation is dominant heat transfer mode and significantly changes the temperature profile throughout the enclosure, the isotherms patterns are concentrated on the hot and cold wall. The streamlines have a circular shape and presents a single vortex. For Pl=0.1 and 100, the isothermal contours are similar and the streamlines display nearly centro-symmetric structure.

Figure 9 shows the Planck number affects the temperature distribution in horizontal and vertical mid-planes. At Pl = 0.001, the radiative transfer is the dominant mode and the temperature inside the enclosure is higher. Pl = 0.1 and 100 temperature distributions are similar. The temperature gradient is more evident in the hot and cold walls.

Figure 10 illustrates the effect of the Planck number on the horizontal and vertical velocity profile along the respective horizontal and vertical mid-planes. When Planck number decreases, the horizontal and vertical velocity magnitude increases. The decrease in the number of Planck indicates that it increases the gradient of temperature and velocity across the active walls and generates a non-stagnant flow enclosure. The radiation effect is stronger and the convection effect is weakened.

In Table 4, for $Ra=10^{10}$, τ=1 and ω=0, the mean total, radiative and convection Nusselt numbers change is seen in different Pl numbers. For τ=1, the mean total and radiative Nusselt numbers decrease with increasing the Planck number, however, the mean convection Nusselt number increases with increasing Planck number.

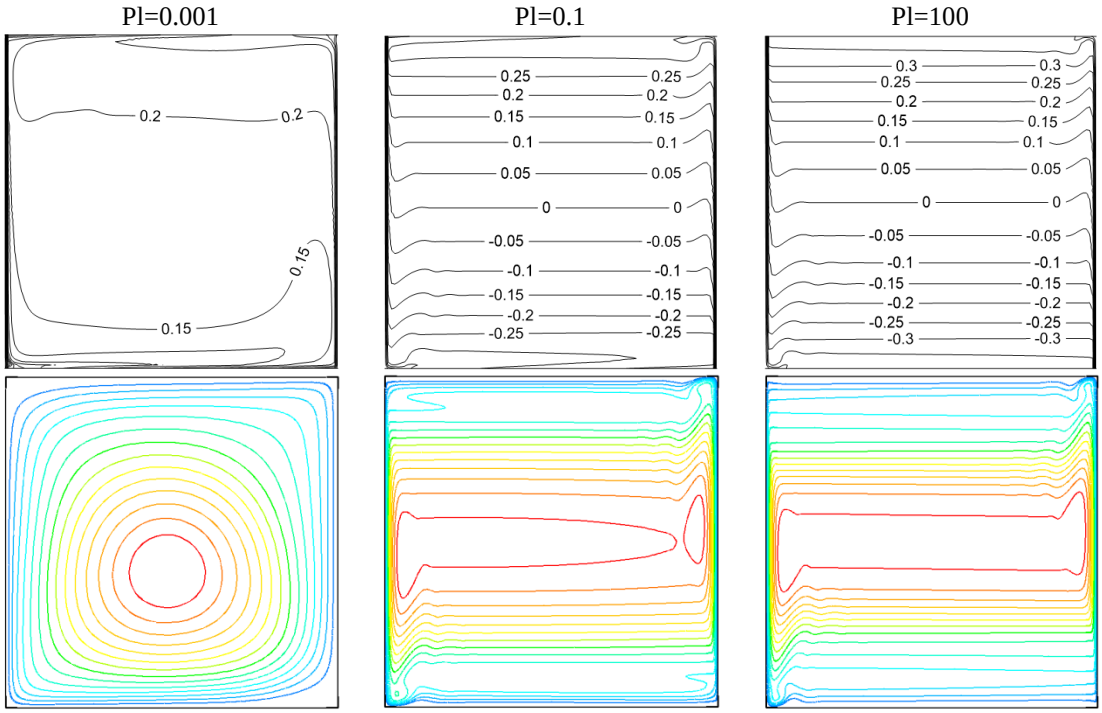

Figure 8. Isotherms (top) and streamlines (bottom) and at Ra=10^{10}, τ=1, ω=0, $\varepsilon_{w1}=\varepsilon_{w2}=\varepsilon_{w3}=\varepsilon_{w4}=1$ and for various Pl numbers.

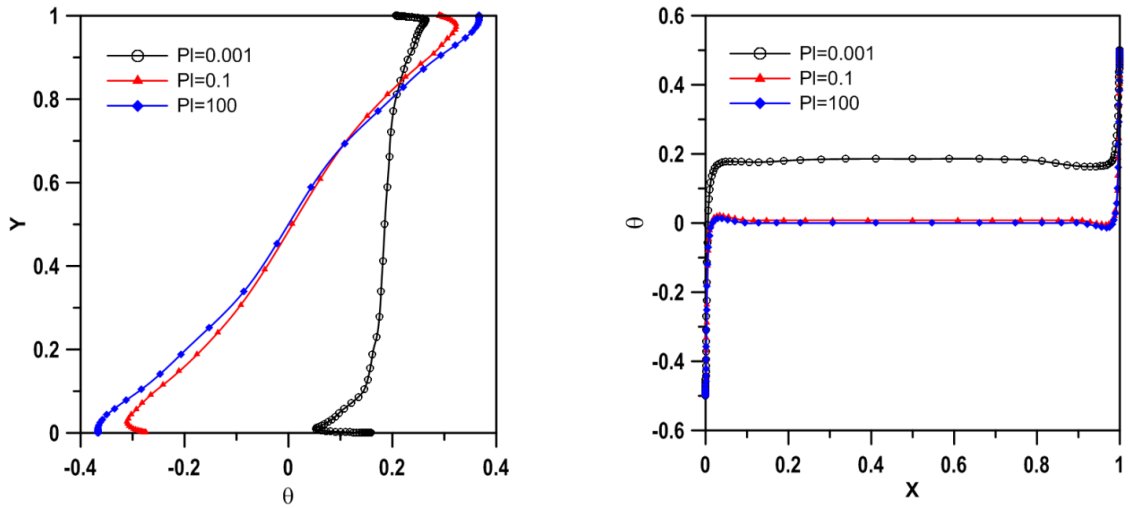

Figure 9. Temperature distribution at X=0.5 mid-plane (left) and Y=0.5 mid-plane (right) for Ra=10^{10}, τ=1, ω=0, $\varepsilon_{w1}=\varepsilon_{w2}=\varepsilon_{w3}=\varepsilon_{w4}=1$.

Table 4. Variation of the mean total, radiative and convection Nusselt number at various Pl number for Ra=10^{10}, τ=1, ω=0, $\varepsilon_{w1}=\varepsilon_{w2}=\varepsilon_{w3}=\varepsilon_{w4}=1$.

Pl	$\overline{Nu_t}$	$\overline{Nu_r}$	$\overline{Nu_c}$
0.0005	830.640	800.616	30.024
0.001	445.837	413.304	32.533
0.1	71.088	5.195	65.892
10	68.100	0.052	68.048
100	68.090	0.005	68.085

Effects of Scattering Albedo Parameter

To investigate the effect of scattering albedo on flow field and temperature distribution for three values of scattering albedo coefficient (ω=0, 0.5 and 1), the following parameter are fixed, namely, Ra=10^{10}, Pl=0.02 for τ=1. Figure 11 displays the effect of the scattering albedo on isotherms and streamlines. The effect of scattering albedo on streamlines is limited and the flow field in the core enclosure expands slightly. However, for ω=1, the streamlines is similar to τ=0 profiles. Additionally, as the scattering albedo increases, the effect of radiative transfer decreases, and the isotherms profiles are very similar.

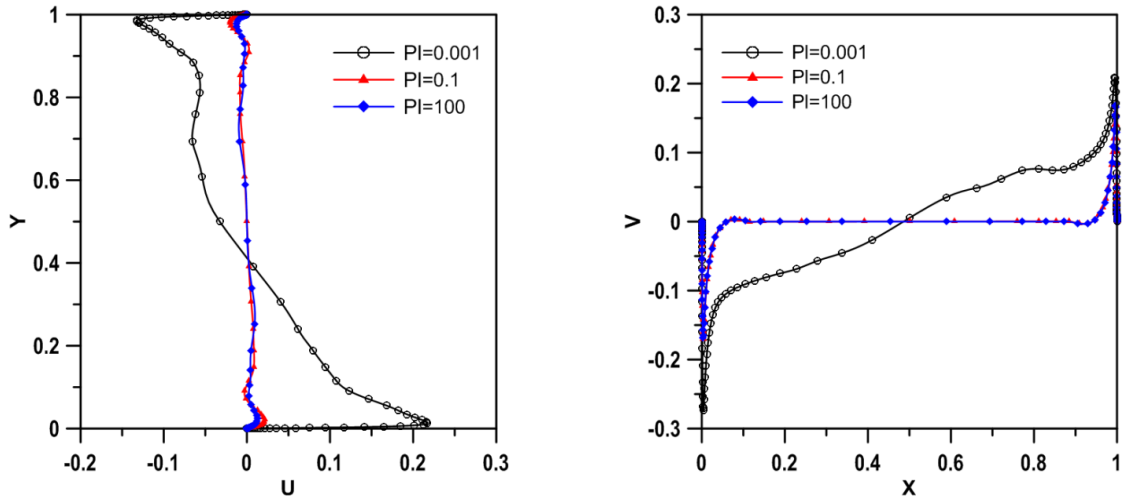

Figure 10. Horizontal velocity at X=0.5 mid-plane (left) and vertical velocity Y=0.5 mid-plane (right) for Ra=10^{10}, τ=1, ω=0, ε_{w1}= ε_{w2}= ε_{w3}= ε_{w4}=1.

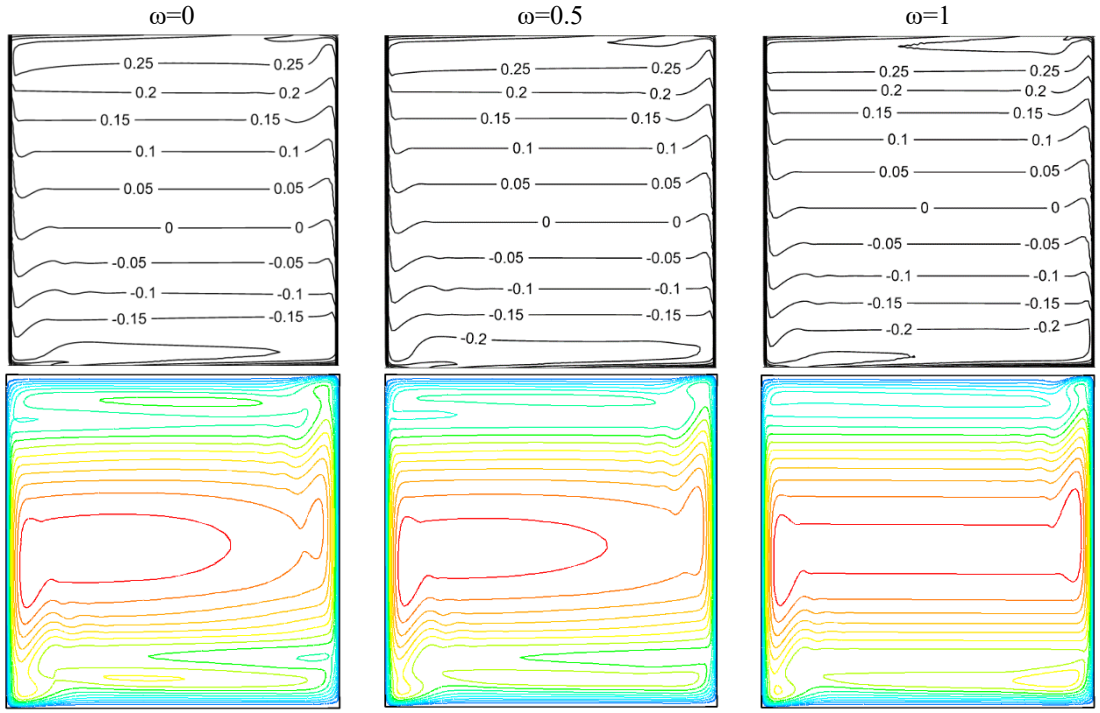

Figure 11. Albedo effect on isotherms (top) and streamlines (bottom) at Ra=10^{10}, Pl=0.02 τ=1, ε_{w1}= ε_{w2}= ε_{w3}= ε_{w4}=1.

Figure 12 displays the dimensionless temperature profiles in the horizontal and the vertical mid-plane for three values of scattering albedo. The temperature profiles seem to be less affected by variations in scattering albedo. When the environment is completely absorbent (ω=0), the temperature is somewhat higher than the others.

Figure 13 depicts the effect of scattering albedo on the horizontal and vertical velocity profile along the respective horizontal and vertical mid-planes. As the scattering albedo increases, the vertical velocity profile remains to be similar. The horizontal velocity magnitude is listed as ω=0, 0.5 and 1, respectively.

Effects of Wall Emissivities

The effect of wall emissivity on total heat transfer is investigated for Ra=10^{10}, Pl=0.02, τ=1 and ω=0, while the wall emissivity can take the values 0, 0.1, 0.5 and 1. Table 5 shows the impact of the wall emissivity in the presence of thermal radiation. For the hot wall (right wall), the increase of wall emissivity leads to the increase of mean total Nusselt number. Additionally, the same trend can be seen for top wall emissivity. However, for cold wall (left wall), the increasing of wall emissivity leads to slightly the decrease of mean total Nusselt number, and there is also the same trend for bottom wall emissivity. Decreasing the emissivity of the hot wall reduces the radiation Nusselt number considerably. Actually, the wall emissivity effects significantly the heat transfer in the enclosure. When the

hot and cold walls are black and the insulated walls are reflected, the maximum heat transfer is obtained.

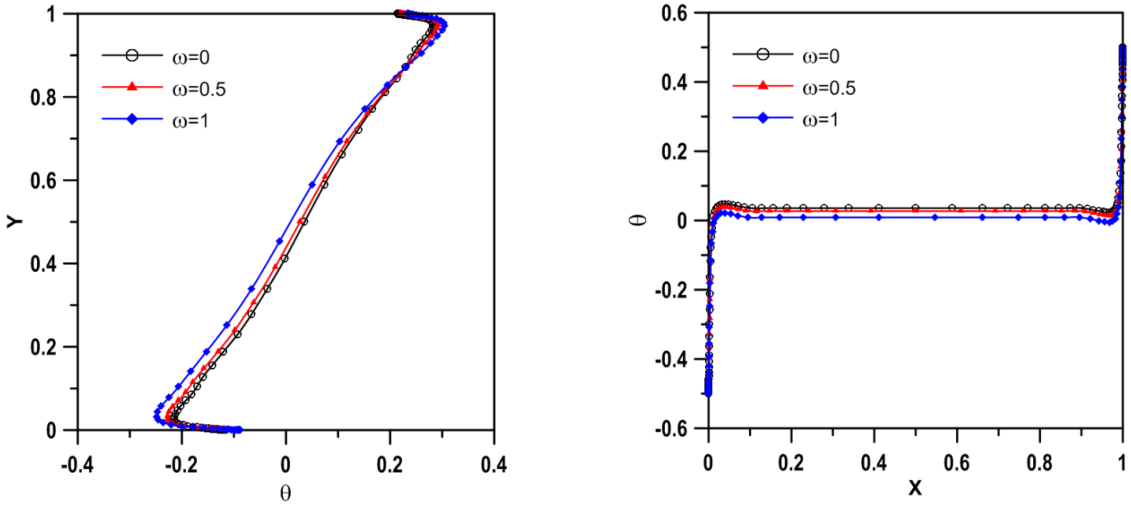

Figure 12. Temperature distribution at X=0.5 mid-plane (left) and Y=0.5 mid-plane (right) for Ra=10^{10}, Pl=0.02, τ=1, $\varepsilon_{w1}=\varepsilon_{w2}=\varepsilon_{w3}=\varepsilon_{w4}=1$.

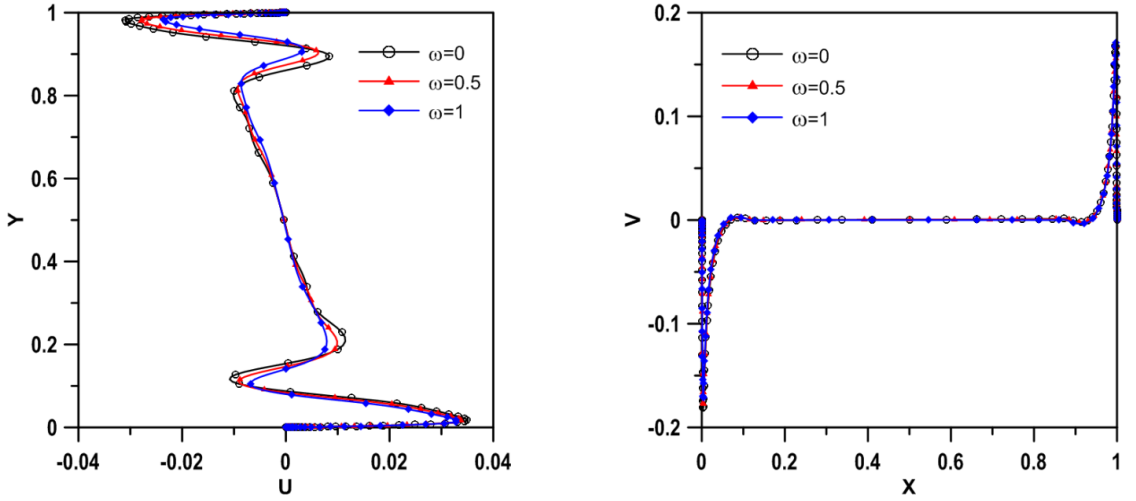

Figure 13. Horizontal velocity at X=0.5 midplane (left) and vertical velocity Y=0.5 midplane (right) for Ra=10^{10}, Pl=0.02, τ=1, $\varepsilon_{w1}=\varepsilon_{w2}=\varepsilon_{w3}=\varepsilon_{w4}=1$.

Table 5. Variation of the mean total, radiative and convection Nusselt number for various wall emissivities.

Wall emissivity				$\overline{Nu_t}$	$\overline{Nu_r}$	$\overline{Nu_c}$
bottom	right	top	left			
0.1	1	1	1	84.830	24.291	60.538
0.5	1	1	1	84.325	24.855	59.470
1	0.1	1	1	70.968	2.758	68.210
1	0.5	1	1	76.936	13.280	63.655
1	1	0.1	1	76.271	22.471	53.800
1	1	0.5	1	79.803	23.804	55.998
1	1	1	0.1	84.403	25.729	58.674
1	1	1	0.5	84.094	25.494	58.600
0	1	0	1	85.507	24.586	60.921
1	1	1	1	83.807	25.303	58.504
0	0	0	0	66.165	0	66.165

CONCLUSION

An investigation has been performed on interactions turbulent natural convective and radiative heat transfer within a differentially heated enclosure with a gray and absorbing, emitting and isotropically scattering medium. The discrete ordinates method is used for radiative transfer calculations. Studies have been carried out for a wide range of influencing parameters such as Rayleigh number, the wall emissivity, the Planck number, optical

thickness and the scattering albedo. The effects of these parameters on flow and heat transfer are encountered in various engineering applications. The effects of the parameters discussed on turbulent natural convection and radiation flow and heat transfer are summarized below.

According to surface radiation, thermal radiation alters the characteristics of flow fields in the enclosure under the thermal boundary conditions considered.

The increase in the Rayleigh number causes an increase in the heat transfer in enclosure. On the other hand, increasing the optical thickness reasons a decrease in the heat transfer for a fixed Rayleigh number and the maximum of heat transfer is occurred for low optical thickness with the presence of thermal radiation. $\overline{Nu_t}$ =87.796 and 82.351 is obtained for τ=0.2 and 5, respectively (Ra=10^{10}, Pl=0.02 and ω=0).

For Pl<0.001, the isotherm lines and the streamlines are considerably altered in enclosure and velocities are intensified by the presence of radiation. The heat transfer increases with decreasing the Planck number. $\overline{Nu_t}$ =445.837 and 68.10 is found for Pl=0.001 and 10, respectively (Ra=10^{10}, τ=1 and ω=0).

The albedo effect on the temperature and velocity distribution is quite limited in the enclosure and radiation effect decreases with the increase of scattering albedo.

For a fixed optical thickness and the Planck number, the decrease in the hot wall emissivity leads to decrease in the heat transfer in enclosure. Especially, radiative heat transfer in hot wall decreases significantly. When the hot and cold walls are black and the adiabatic walls are reflected, the maximum heat transfer ($\overline{Nu_t}$ =85.507) is obtained for Ra=10^{10}, Pl=0.02, τ=1 and ω=0.

REFERENCES

Capdevila R., Lehmkuhl O., Trias F.X., Pérez-Segarra C.D. and Colomer G., 2011, Turbulent natural convection in a differentially heated cavity of aspect ratio 5 filled with non-participating and participating grey media, *J Phys: Conf Series*, 318: 042048.

Capdevila R., Lehmkuhl O., Colomer G. and Perez-Segarra C.D, 2012, Study of turbulent natural convection in a tall differentially heated cavity filled with either non-participating, participating grey and participating semigrey media, *J. Phys: Conf Series*, 395: 1-8.

Czarnota T. and Wagner C., 2016, Turbulent convection and thermal radiation in a cuboidal Rayleigh–Bénard cell with conductive plates, *Int J Heat Fluid Fl*, 57, 150–72.

Desrayaud G. and Lauriat G., 1985, Natural convection of a radiating fluid in a vertical layer, *J Heat Transf*, 107, 710–2.

Draoui A., Francis A. and Beghein C.,1991, Numerical analysis of heat transfer by natural convection and radiaition in participating fluids enclosured in square cavities, *Numer. Heat Transfer, Part A*, 20, 253–61.

Fluent User's Guide, Fluent Inc., USA; 2011.

Fusegi T. and Farouk B., 1989, Laminar and turbulent natural convection-radiation interaction in a square enclosure filed with a nongray gas, *Numer. Heat Transfer, Part A*, 15, 303-22.

Ibrahim A., Saury D. and Lemonnier D., 2013, Coupling of turbulent natural convection with radiation in an air-filled differentially-heated cavity at Ra = 1.5 x 10^9, *Comput Fluids*, 88, 115–25.

Lauriat G., 1982, Combined radiation–convection in gray fluids enclosed in vertical cavities, *J Heat Transf*, 104, 609–15.

Mesyngier C. and Farouk B., 1996, Turbulent natural convection-nongray gas radiation analysis in a square enclosure, *Numer. Heat Transf Part A*, 29, 671–87.

Mezrhab A., Lemonnier D., Meftah S. and Benbrik A., 2008, Numerical study of double diffusion convection coupled to radiation in a square cavity filled with a participating grey gas, *J Phys D: Appl Phys*, 41, 195501–17.

Miroshnichenko I.V., Sheremet M.A. and Mohamad A.A., 2016, Numerical simulation of a conjugate turbulent natural convection combined with surface thermal radiation in an enclosure with a heat source, *Int J Therm Sci*, 109, 172–81.

Mondal B. and Mishra S.C., 2009, Simulation of natural convection in the presence of volumetric radiation using the lattice Boltzmann method, *Numer. Heat Transfer, Part A*,55, 18–41.

Moufekkir F., Moussaoui M.A., Mezrhab A., Naji H. and Lemonnier D.,2012, Numerical prediction of heat transfer by natural convection and radiation in an enclosure filled withan isotropic scattering medium, *J Quant Spectrosc Radiat Transf*, 113, 1689-1704.

Moufekkir F., Moussaoui M.A., Mezrhab A., Lemonnier D. and Naji H., 2012, MRT-lattice Boltzmann computations of natural convection and volumetric radiation in a tilted square enclosure, *Int J Therm Sci*, 54, 124-141.

Salat J., Xin S., Joubert P., Sergent A., Penot F. and Quéré P.L., 2004, Experimental and numerical

investigation of turbulent natural convection in a large air-filled cavity, *Int J Heat Fluid Fl*, 25, 824–32.

Sergent A., Xin S., Joubert P., Quéré P.L., Salat J. and Penot F., 2013, Resolving the stratification discrepancy of turbulent natural convection in differentially heated air-filled cavities – Part I: reference solutions using Chebyshev spectral methods, *Int J Heat Fluid Fl*, 39, 1–14.

Sharma A.K, Velusamy K., Balaji C. and Venkateshan S.P., 2007, Conjugate turbulent natural convection with surface radiation in air filled rectangular enclosures, *Int J Heat Mass Transf*, 50, 625–39.

Sharma A,K., Velusamy K. and Balaji C., 2008, Interaction of turbulent natural convection and surface thermal radiation in inclined square enclosures, *Heat Mass Transf*, 44, 1153–70.

Shati A.K.A, Blakey S.G. and Beck S.B.M., 2012, A dimensionless solution to radiation and turbulent natural convection in square and rectangular enclosures, *J Eng Sci Techn*, 7 (2), 257–79.

Sheremet M,A. and Miroshnichenko I.V, 2015, Numerical study of turbulent natural convection in a cube having finite thickness heat-conducting walls, *Heat Mass Transf*, 51, 1559–69.

Soucasse L., Riviere P., Soufiani A., Xin S. and Quéré P.L., 2014, Transitional regimes of natural convection in a differentially heated cubical cavity under the effects of wall and molecular gas radiation, *Phys. Fluids*, 26, 024105-1–23.

Tan Z. and Howell J.R., 1991, Combined radiation and natural convection in a square enclosure with participating medium, *Int J Heat Mass Transf*, 34, 79–97.

Velusamy K., Sundararajan T. and Seetharamu K.N., 2001, Interaction effects between surface radiation and turbulent natural convection in square and rectangular enclosures, *J Heat Transf*, 123 (6), 1062–70.

Webb B.W. and Viskanta R., 1987, Radiation-induced buoyancy driven flow in rectangular enclosures: Experiment and analysis, *J Heat Transf*, 109, 427–33.

Wu T. and Lei C., 2015, On numerical modelling of conjugate turbulent natural convection and radiation in differentially heated cavity, *Int J Heat Mass Transf*, 91, 454–66.

Xamán J., Arce J., Álvarez G. and Chávez Y., 2008, Laminar and turbulent natural convection combined with surface thermal radiation in a square cavity with a glass wall, *Int J Therm Sci*, 47, 1630–8.

Xin S., Salat J., Joubert P., Sergent A., Penot F. and, Quéré P.L., 2013, Resolving the stratification discrepancy of turbulent natural convection in differentially heated air-filled cavities. Part III: a full convection–conduction–surface radiation coupling, *Int J Heat Fluid Fl*, 42, 33–48.

Yucel A. and Acharya S., and Williams M.L., 1989, Natural convection and radiation in a square enclosure, *Numer. Heat Transfer, Part A*, 15, 261–78.

Yucel A. and Acharya S., and Williams M.L., 1994, Natural convection of a radiating fluid in square enclosure with perfectly conducting end walls, *Sadhana*, 519, 751–64.

Mesut TEKKALMAZ was born in Eskişehir-Turkey in 1972. He graduated from Department of Mechanical Engineering of Eskişehir Anadolu University in 1994. He received the degree of MSc and PhD from Department of Mechanical Engineering of Eskişehir Osmangazi University in 1996 and 2003, respectively. He received the title of Associate Professor in 2014 and Professor in 2019. He is currently working at Department of Mechanical Engineering of Eskişehir Osmangazi University. He is married and has one child.